LANGMUIR

pubs.acs.org/Langmuir Article

Molecular Orientation and Energy Transfer Dynamics of a Metal Oxide Bound Self-Assembled Trilayer

Dhruba Pattadar, Ashley Arcidiacono, Drake Beery, Kenneth Hanson,* and S. Scott Saavedra*

Cite This: *Langmuir* 2023, 39, 10670−10679 Read Online

ACCESS | Metrics & More | Article Recommendations | Supporting Information

ABSTRACT: Self-assembly of molecular multilayers via metal ion linkages has become an important strategy for interfacial engineering of metalloid and metal oxide (MO_x) substrates, with applications in numerous areas, including energy harvesting, catalysis, and chemical sensing. An important aspect for the rational design of these multilayers is knowledge of the molecular structure−function relationships. For example, in a multilayer composed of different chromophores in each layer, the molecular orientation of each layer, both relative to the adjacent layers and the substrate, influences the efficiency of vectorial energy and electron transfer. Here, we describe an approach using UV−vis attenuated total reflection (ATR) spectroscopy to determine the mean dipole tilt angle of chromophores in each layer in a metal ion-linked trilayer self-assembled on indium-tin oxide. To our knowledge, this is the first report demonstrating the measurement of the orientation of three different chromophores in a single assembly. The ATR approach allows the adsorption of each layer to be monitored in real-time, and any changes in the orientation of an underlying layer arising from the adsorption of an overlying layer can be detected. We also performed transient absorption spectroscopy to monitor interlayer energy transfer dynamics in order to relate structure to function. We found that near unity efficiency, sub-nanosecond energy transfer between the third and second layer was primarily dictated by the distance between the chromophores. Thus, in this case, the orientation had minimal impact at such proximity.

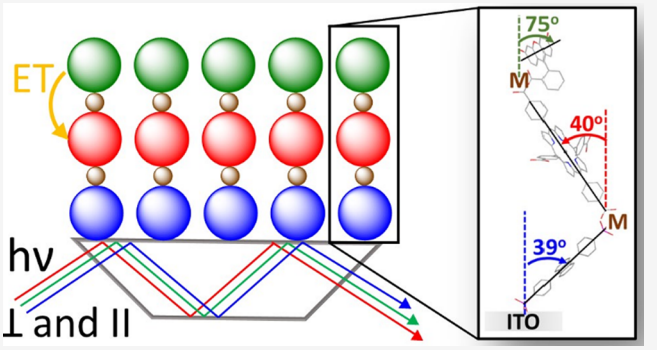

INTRODUCTION

Modification of metalloid and metal oxide (MO_x) substrates with organic monolayers to alter their interfacial properties has a long history and applications in many fields, such as organic electronics,[1−3] chemical and biosensing,[4,5] dye-sensitized solar energy conversion,[6] and control of protein adsorption and cell adhesion.[7−9] More recently, strategies to self-assemble molecular multilayers via metal ion linkages have emerged,[3] where the different components of each layer[10] provide for more nuanced control and enable interfacial engineering of energy harvesting, photoinduced charge separation, vectorial electron/energy transfer, etc.[11,12] The metal ion-linked multilayer assembly strategy has been employed to generate bilayers for energy/electron cascade solar cells[13−15] and photoelectrosynthesis cells,[16,17] trilayers for triplet−triplet annihilation upconversion (TTA-UC),[12,18] H_2 evolution catalysis,[19] and molecular p-n junctions,[20,21] and even >4 layers for electrochemiluminescent dopamine detection[22] and electrochromism.[23]

An important aspect for the rational design of these assemblies is knowledge of molecular structure−function relationships, i.e., controlling the structure of each layer is a prerequisite to obtaining their desired function(s). For example, the rate and efficiency of interlayer energy transfer are directly dependent on the distance and orientation between the donor and acceptor chromophores, as dictated by the position of the metal ion binding motif.[11,24] Likewise, electron transfer between molecular layers and an electrode substrate can be enhanced or inhibited using strategic selection of the metal ion, molecular components, and substrate porosity.[25−29]

Given the importance of structure, the focus of this paper is the determination of molecular orientation of each layer in a self-assembled trilayer, both relative to adjacent layers and relative to a MO_x substrate. Various experimental techniques have been implemented to determine the tilt angle of molecules deposited on MO_x substrates. Examples include X-ray reflectometry (XRR),[30,31] near edge X-ray absorption fine structure (NEXAFS),[32,33] polarized infrared reflection absorption spectroscopy (IRRAS),[32,34,35] UV−vis attenuated total reflection (ATR) spectrocopy,[36,37] sum-frequency vibrational

Received: May 17, 2023
Revised: June 24, 2023
Published: July 19, 2023

spectroscopy,[38] and two-photon photoelectron spectroscopy.[39] In most cases, applying these techniques to multi-chromophore systems is challenging due to overlapping signals. For example, it is difficult to obtain layer-specific information using NEXAFS because of the lack of a spectrally resolved contribution from each layer. In contrast, layer-specific information can be obtained using UV−vis ATR, as we have previously demonstrated.[11] In that study, we measured the mean tilt angles of two different chromophores in a metal ion linked bilayer: the first layer was a diphenyl anthracene diphosphonic acid (**A**) adsorbed on indium-tin oxide (ITO), and the second layer was a carboxy Pt-porphyrin derivative (**P**) that was linked to the first layer through a coordinated Zn^{2+}.

Recently Zhou et al. described a self-assembled trilayer (MO_x-**A**-Zn-**P**-Zn-**F**) for more efficient TTA-UC solar cells,[12] containing a photoanode composed of the aforementioned **A**-Zn-**P** bilayer capped with a metal ion linked, carboxy fluorescein (**F**) layer (Figure 1). This system is remarkable in that spectroscopic measurements indicate that it can facilitate **F** to **P** and **P** to **A** energy transfer, TTA between adjacent **A** molecules, electron transfer from **A** to the MO_x substrate, and regeneration via an electron transfer cascade, all while suppressing undesirable back energy transfer events (**P** to **F** and **A** to **P**). The strong dependence of structure on each of these dynamic processes prompted the structural characterization described herein. We detail a methodology to determine the molecular orientation of each layer in the **A**-Zn-**P**-Zn-**F** trilayer self-assembled on ITO. Measuring the mean tilt angle of each layer in a trilayer composed of three different chromophores is unprecedented and offers insight into the role of molecular orientation and its impact on interlayer dynamics, as measured by transient absorption spectroscopy, in surface-confined TTA-UC assemblies.

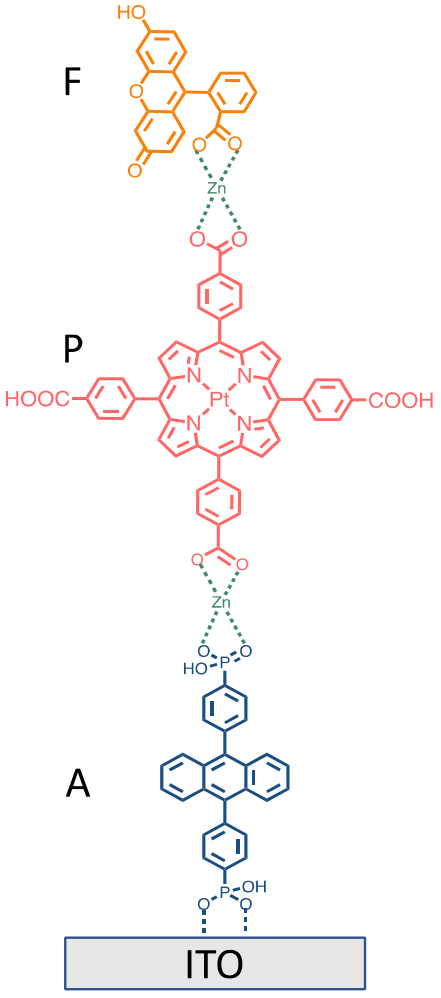

Figure 1. Chemical structure of the **A**-Zn-**P**-Zn-**F** trilayer on ITO. Bidentate binding of the phosphonic and carboxylic acids is assumed but not verified.

EXPERIMENTAL SECTION

Materials. Zinc acetate dihydrate (99.99%), poly-L-lysine hydrobromide (mol wt 30,000−70,000), dimethyl sulfoxide (DMSO) (anhydrous, ≥99.9%), 2-propanol, hexane, sodium phosphate dibasic (ACS reagent, ≥99.0%), sodium phosphate monobasic (ACS reagent, ≥99.0%), fluorescein sodium salt (**F**), Sephadex G-25, and Triton-X were purchased from Sigma Aldrich. Ethanol (200 proof) was purchased from Decon Labs. AZDye 405 NHS Ester (405 dye) was purchased from Fluoroprobes. Pt(II) meso-tetra(4-carboxyphenyl)-porphine (**P**) was purchased from Frontier Scientific. Dextran-rhodamine B (10,000 M_w) was purchased from ThermoFisher Scientific. 4,4′-(anthracene-9,10-diyl)bis(4,1-phenylene) diphosphonic acid (A) was synthesized following previously published procedures.[40,41] Glass slides coated with indium tin oxide were purchased from Thin Film Devices (1 mm thick glass; ITO layer thickness of 145 nm; sheet resistance of 20−30 Ω/sq).

Labeling Poly(lysine) with 405 NHS Ester. Poly(lysine) was labeled with 405 dye following a published protocol.[42] Briefly, 2 mg of 405 dye was dissolved in 200 μL of DMSO, and 10 mg of poly(lysine) was dissolved in 1.8 mL of phosphate buffer (pH 8.3−8.5) with stirring. The 405 dye solution was added dropwise to the poly(lysine) solution and stirred for 5 h. The unreacted dye was separated from the product, poly(lysine)-405 dye, using a desalting column packed with Sephadex G-25 resin.

Substrate Cleaning Procedure. ITO slides were cleaned by scrubbing with 1% Triton X-100 followed by sonicating sequentially in 1% Triton X-100, nanopure water (18.1 MΩ cm), hexane, acetone, and isopropyl alcohol (20 min each) and then stored in ethanol. Immediately before use, slides were rinsed with ethanol and dried under N_2.

Attenuated Total Reflectance (ATR) Spectroscopy. A custom-built, UV−vis ATR spectrometer was used to measure polarized ATR spectra of **A**, **P**, and **F** films assembled on ITO-coated slides. The ATR spectrometer is described in previous papers.[43−45] Briefly, a collimated broadband source (Xe lamp) was coupled into and out of the waveguide (an ITO-coated slide) using two BK7 prisms (n = 1.51). The light exiting the waveguide was directed into a monochromator (Newport MS260i) and detected using a CCD detector (Andor iDus420A). The two prisms were placed 44.5 mm apart producing eight total internal reflections at the ITO/solution interface. The total internal reflection angle in the waveguide was ∼74°. A Glan−Thompson polarizer was used to select either transverse magnetic (TM) or transverse electric (TE) polarization. A liquid flow cell was used to introduce dissolved dye molecules to the waveguide surface and, after the formation of the adsorbed film, non-adsorbed dyes were flushed out. Adsorption isotherms measured with TM polarized light were used to establish the conditions (listed in Table S1) for preparing films for molecular orientation measurements. Baseline shifts in ATR spectra, if they occurred, were corrected by normalizing spectra over the wavelength range of 300−330 nm. Three-point smoothing was applied to all spectra before analysis.

Dichroic ratios for **A**, **P**, and **F** films were determined from the respective polarized ATR spectra, and mean dipole tilt angles of the films were determined from their respective dichroic ratios, as described in previous publications.[11,36,43] A correction for the unequal interfacial electric field intensities in TM and TE polarizations was implemented following the method of Mendes et al.[46] For **A** films, the intensity difference was normalized by measuring the dichroic ratio of

https://doi.org/10.1021/acs.langmuir.3c01323
Langmuir 2023, 39, 10670−10679

a poly(lysine)-405 dye film adsorbed on a waveguide. For **P** and **F** films, the intensity difference was normalized by measuring the dichroic ratio of a dextran-rhodamine B film adsorbed on a waveguide. It was assumed that the 405 dye and rhodamine B moieties were randomly oriented in these films. The preparation conditions and the wavelength integration ranges for **A**, **P**, **F**, poly(lysine)-405 dye, and dextran-rhodamine B films are given in Table S1. Example dichroic spectra of poly(lysine)-405 dye and dextran-rhodamine B films are shown in Figure S1.

The surface coverage (Γ) of adsorbed **A**, **P**, and **F** films was estimated from[11,47]

$$\Gamma = A_f\,[1000N\varepsilon_f\,(I_e/I_i)]^{-1} \quad (1)$$

where A_f is the absorbance of the respective film measured in TM polarization, ε_f is the molar absorptivity of the dye in the film (assumed to be equal to ε_b, the molar absorptivity of the dissolved dye), N is the number of total internal reflections, and I_e/I_i is evanescent transmitted interfacial intensity per unit incident intensity. I_e/I_i was calculated using the two-phase approximation,[48] using refractive indices of $n_1 = 1.36$ (for ethanol) or 1.33 (for water) for the superstrate medium, $n_2 = 1.52$ (at wavelengths <500 nm) or 1.51 (at wavelengths >500 nm) for the glass slide, and ignoring the metal oxide layer and the adsorbed molecular film. For **A**, **P**, and **F**, the measured ε_b values were 12,200 M^{-1} cm^{-1} at 395 nm, 27,200 M^{-1} cm^{-1} at 511 nm, and 23,600 M^{-1} cm^{-1} at 497 nm, respectively. Ignoring the ITO layer in the I_e/I_i calculation introduces a systematic error in the estimated Γ values; however, the error is the same for each film, so the estimates are accurate on a relative basis, enabling them to be compared. Assuming $\varepsilon_f = \varepsilon_b$ may also introduce error if the absorbance spectra of the dissolved and adsorbed chromophore are significantly different, which was the case for **A** (see below). It is unlikely, however, that ε_f and ε_b differ by more than 2-fold, and again we emphasize that the Γ values are estimates used only for relative comparison.

Mesoporous Sample Preparation. ZrO_2 paste was synthesized using previously published procedures.[40,49] Films were generated using the doctor blade method onto glass substrates and sintered. The glass was then cut into 2 cm × 2 cm squares. SEM images of mesoporous ZrO_2 films are shown in Wang et al.[29] Bilayers of **P** and **F** were produced by immersing cut films in 200 μM **P** in DMSO for 6 h, then $Zn(CH_3COO)_2$ for 2 h, and 300 μM **F** in MeOH for 30 min, as previously described.[12]

Transient Absorption. Transient absorption measurements were conducted using a HELIOS FIRE transient absorption spectrometer (Ultrafast Systems) in conjunction with a Vitara-S Coherent Ti:sapphire laser with amplification via a 1 kHz Coherent Revolution-50 pump laser. The resulting pulse (5 mJ, 100 fs full-width half max at 800 nm) was then separated into a pump and probe beam. The pump was then directed through an optical parametric amplifier (OPeraA Solo, Coherent), after which the light was chopped to reduce laser line scattering in full spectra analysis. The probe was directed through the delay stage to a white light continuum crystal (sapphire) for white light probe production. The pump beam was then overlapped with the probe on the film or solution in a clamp stage. Solutions were stirred during measurement, while film samples were rastered to avoid bleaching and localized heating effects. The signal was then collected by a CMOS detector. Difference spectra and single wavelength kinetics were acquired using 0.01 ps exponential steps for 3 averages over 2 s. Chirp correction and background correction were performed with the Surface Xplorer software package. Single wavelength kinetics were fitted with a biexponential function, and a weighted average was calculated using eqs 2 and 3, respectively,

$$y = A_1 e^{-k_1 x} + A_2 e^{-k_2 x} + y_0 \quad (2)$$

$$\tau_i = \frac{1}{k_i};\ \langle\tau\rangle = \sum A_i\tau_i^2 / \sum A_i\tau_i \quad (3)$$

where k is the rate constant, τ is the lifetime $(1/k)$, and A_n is the amplitude of a given component.

RESULTS AND DISCUSSION

Trilayer Formation and Structure. Polarized ATR spectroscopy was used to monitor the formation and characterize the structure of each chromophore layer in the **A**-Zn-**P**-Zn-**F** trilayer (Figure 1). Major advantages of the ATR approach include: (a) the multiple internal reflection ATR geometry is much more sensitive than a transmission geometry, and (b) measurements can be made in both TE and TM polarizations, from which the mean out-of-plane tilt angle of an ensemble of absorption dipoles can be determined. The experimental procedure and example data from one trial are presented below, and results from multiple trials are listed in Table 1.

Table 1. Mean Tilt Angles of A, P, and F in Monolayer, Bilayer, and Trilayer Films on ITO

chromophore	mean tilt angle (°)[a]	surface coverage × 10^{-10} (mol/cm^{-2})[a]
A (in **A** film)	31 ± 3	3.6 ± 0.55
A (in **A-Zn** film)	33 ± 2	
A (in **A-Zn-P** film)	38 ± 2	
P (in **A-Zn-P** film)	37 ± 3	2.8 ± 0.82
P (in **A-Zn-P-Zn** film)	40 ± 4	
A (in **A-Zn-P-Zn-F** film)	39 ± 2	
P (in **A-Zn-P-Zn-F** film)	40 ± 4	
F (in **A-Zn-P-Zn-F** film)	75 ± 5	0.9 ± 0.11

[a]From $n = 3$ trials.

ATR spectral data acquired during the adsorption of **A** from a 40 μM ethanol solution onto ITO are shown in Figure 2A,B. The absorbance increased rapidly, reaching a near steady-state condition after 15−20 min. After 60 min, the cell was flushed with ethanol to remove dissolved and weakly bound molecules. The accompanying minor decline in absorbance is consistent with past studies showing that the phosphonic acid group adsorbs strongly on ITO.[1,50] TE- and TM-polarized ATR spectra of the adsorbed **A** film were then recorded (Figure 2C). Two major bands were observed, centered at ∼379 and ∼395 nm. In contrast, the transmission spectrum of dissolved **A** contained four peaks at 337, 354, 372, and 392 nm wavelength (Figure S2A). Relative to the solution-phase spectrum, the two lower energy peaks in the ATR spectra were broadened and slightly red-shifted (3−7 nm; ∼50 meV), while the two higher energy peaks were notably less pronounced, likely due to inhomogeneous broadening and/or aggregation, which has been reported previously for phosphonic acid-functionalized dyes adsorbed on ITO.[11,36,37]

The dichroic ratio of the adsorbed **A** film was calculated by integrating the TE- and TM-polarized ATR spectra over the wavelength ranges listed in Table S1, and the mean dipole tilt angle, θ_A, was obtained from the dichroic ratio, as described previously.[11,36,43] θ_A is the angle between the linear transition dipole of **A** (aligned along the anthracene short axis through the 9,10-carbon atoms) and the surface normal to ITO substrate.[11,51] The result, 31° (±3°), agrees with our prior measurement of 29° (±5°) as well as studies of other aromatic, phosphonic acid-modified molecules adsorbed on ITO, and other metal oxide substrates.[1,52] The estimated surface coverage of **A** was 3.6 (±0.55) × 10^{-10} mol/cm^{-2}, which is approximately one monolayer (ML) on an atomically flat substrate.[11] However, since the rms surface roughness of the

https://doi.org/10.1021/acs.langmuir.3c01323
Langmuir 2023, 39, 10670−10679

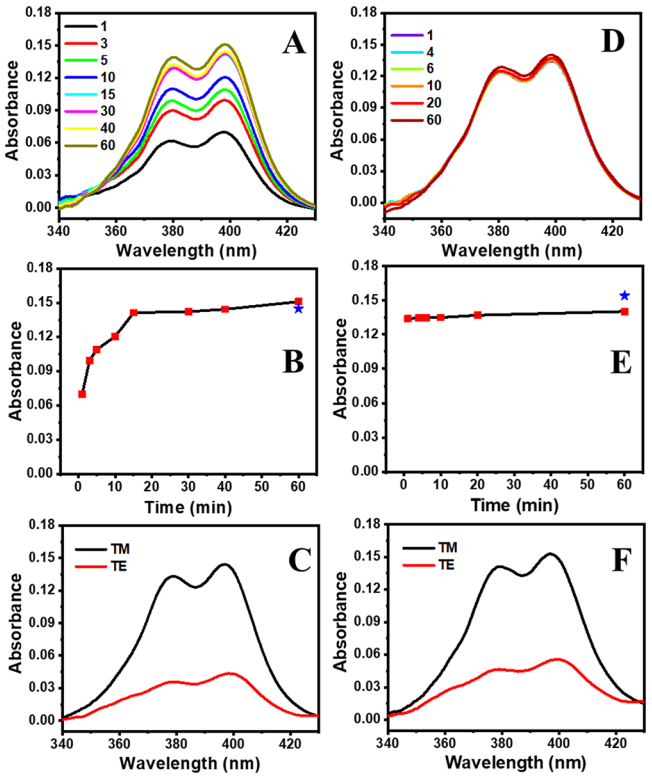

Figure 2. (A) TM-polarized ATR spectra acquired during the adsorption of **A** on ITO. The legend indicates the number of minutes that the **A** solution was incubated with the ITO surface before the spectrum was acquired. (B) Absorbance at 397 nm vs time obtained from the spectra in (A). The blue star is the absorbance after the cell was flushed with fresh ethanol. (C) TM- and TE-polarized ATR spectra of the adsorbed **A** film after the cell was flushed with fresh ethanol. (D) TM-polarized ATR spectra acquired during the adsorption of Zn^{2+}. The legend indicates the number of minutes that the Zn^{2+} solution was incubated with the adsorbed **A** film before the spectrum was acquired. (E) Absorbance at 397 nm vs time obtained from the spectra in (D). The blue star is the absorbance after the cell was flushed with fresh ethanol. (F) TM- and TE-polarized ATR spectra of the adsorbed **A**-Zn film after the cell was flushed with fresh ethanol.

ITO is about 0.5 nm,[53] the actual surface coverage is slightly less than one ML.

ATR spectra were then acquired during the incubation of the **A** film with 100 μM zinc acetate in ethanol (Figure 2D,E). In line with previous reports,[11] minimal changes in the absorbance of **A** (340−440 nm) were observed upon Zn^{2+} coordination, presumably due to the geometric and electronic separation between the chromophore core and the phosphonic acid metal ion binding group. After flushing the flow cell with ethanol, TE- and TM-polarized spectra of the **A**-Zn film were measured (Figure 2F). A θ_A of 33° (±2°) was obtained, which indicates that Zn^{2+} adsorption had no measurable effect on the **A** layer structure.

Figure 3A,B shows spectral data acquired during the incubation of a **P** solution (50 μM in ethanol) with the **A**-Zn film. **P** adsorption reached a steady-state after ∼50 min. At 60 min, the cell was flushed with ethanol, then TE- and TM-polarized ATR spectra of the film were collected (Figure 3C). Two major bands centered at ∼509 and ∼538 nm were observed, which is consistent with the absorbance spectrum of **P** in ethanol solution (Figure S2B). In a control experiment, the adsorption of **P** directly on an **A** film was attempted (i.e., the zinc acetate step was bypassed). In the absence of Zn^{2+}, **P** adsorption did not occur, showing that Zn^{2+} coordination is necessary to link **P** to **A**.

The mean tilt angle of the porphyrin plane of **P**, θ_P, was obtained from the dichroic ratio, as described previously, assuming a circularly polarized dipole.[54,55] The result, 37° (±3°), is in good agreement with our prior measurement of 41° (±6°).[11] A significant difference is the estimated surface coverage of **P**, which here was 2.8 (±0.82) × 10^{-10} mol/cm^{-2}, approximately 1 ML, but only 0.26 (±0.05) × 10^{-10} mol/cm^{-2} in the prior study. This difference is attributed to the two-fold higher concentration of the **P** solution used here. The incubation of the **A**-Zn-**P** bilayer with 100 μM zinc acetate caused no significant changes in the spectra (Figure 3D−F) or the θ_P, which was measured to be 40° (±4°).

To determine the tilt angle of **A** in the **A**-Zn-**P** bilayer, the spectral contribution of **P** in the 360−450 nm range was subtracted from the **A**-Zn-**P** spectrum, yielding the spectrum of **A**-Zn. The coordination of **P** to the **A**-Zn film led to an increase in θ_A from 33° (±2°) to 38° (±2°). This is attributed to the larger projected area of **P** vs **A** which appears to force the **A** molecules to adopt a larger (more in-plane) tilt angle.[11]

ATR spectral data acquired during the incubation of a **F** solution (50 μM in ethanol) with the **A**-Zn-**P**-Zn are shown in Figure 4A,B. The adsorption of **F** reached a steady-state after ∼10 min although the process was allowed to proceed for 60 min. The cell was then flushed with ethanol and TE- and TM-polarized ATR spectra were acquired (Figure 4C). The amount of **F** desorption during flushing was significantly greater than that observed for **A** and **P**. This is likely due to weaker binding arising from steric hindrance between the COOH binding group and the xanthene ring of **F**. When an **F** solution was incubated with a **A**-Zn-**P** film, adsorption did not occur, showing that Zn^{2+} coordination is necessary for **F** to bind to the **A**-Zn-**P**-Zn film. The absorbance spectrum of dissolved **F** shows three bands with maxima at 424, 456, and 494 nm (Figure S2C). The 494 and 424 nm bands are also present in the ATR spectrum of the **F** film, albeit broadened, along with a shoulder at ∼464 nm. As noted above, the band broadening and spectral shift are indicative of inhomogeneous broadening.

The mean dipole tilt angle of the **F** film, θ_F, obtained from the dichroic ratio was 75° (±5°). The estimated surface coverage of **F** was 0.9 (±0.11) × 10^{-10} mol/cm^{-2}, about 0.5 ML and three-fold lower relative to **P** (2.8 × 10^{-10} mol/cm^{-2}). The lower **F** surface coverage may be due to a combination of steric hindrance arising from the COOH binding group located at the ortho position of **F**, adjacent to the xanthene ring, and a decrease in metal ion binding sites with each subsequent layer. The tilt angles of **A** and **P** in the **A**-Zn-**P**-Zn-**F** trilayer were determined by spectral subtraction, as described above. The respective angles were 39° (±2°) and 40° (±4°), showing that the deposition of the **F** layer did not measurably alter the structure of the underlying layers.

A summary of the tilt angle data for **A**, **P**, and **F** at each stage of the trilayer assembly, along with surface coverages, is provided in Table 1. Based on these data, a depiction of the molecular orientations (relative to the ITO surface normal) for the **A**, **A**-Zn-**P**, and **A**-Zn-**P**-Zn-**F** films are shown in Figure 5. As noted above, the tilt angles for **A** and **P** are depicted using the transition dipole across the 9,10-carbon atoms of the anthracene core[11,51] and in the plane of the porphyrin,

https://doi.org/10.1021/acs.langmuir.3c01323
Langmuir 2023, 39, 10670−10679

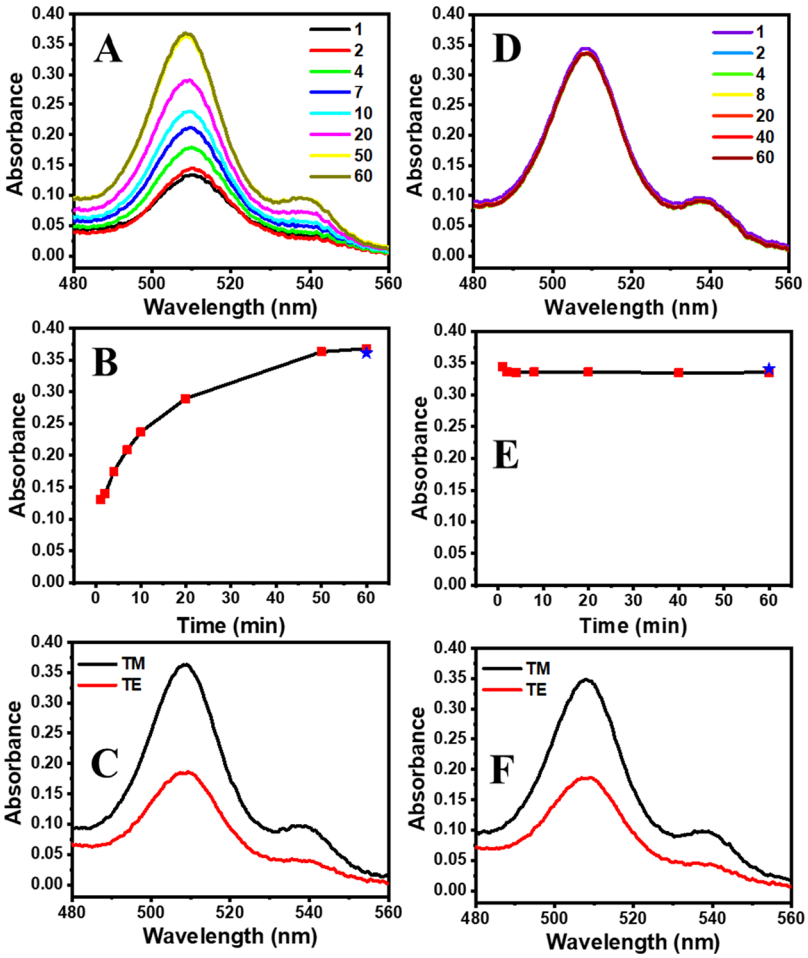

Figure 3. (A) TM-polarized ATR spectra were acquired during the adsorption of **P** to the **A**-Zn film, as shown in Figure 2. The spectra were blanked against the spectrum of the **A**-Zn film recorded before the **P** solution was injected into the flow cell. The legend indicates the number of minutes that the **P** solution was incubated with the **A**-Zn film before the spectrum was acquired. (B) Absorbance at 509 nm vs time obtained from the spectra in (A). The blue star is the absorbance after the cell was flushed with fresh ethanol. (C) TM- and TE-polarized ATR spectra of the **P** layer of the **A**-Zn-**P** film after the cell was flushed with fresh ethanol. (D) TM-polarized ATR spectra were acquired during the adsorption of Zn^{2+}. The spectra were blanked against the spectrum of the **A**-Zn film recorded before the **P** solution was injected into the flow cell. The legend indicates the number of minutes that the Zn^{2+} solution was incubated with the adsorbed **A**-Zn-**P** film before the spectrum was acquired. (E) Absorbance at 509 nm vs time obtained from the spectra in (D). The blue star is the absorbance after the cell was flushed with fresh ethanol. (F) TM- and TE-polarized ATR spectra of the **P**-Zn layer of the **A**-Zn-**P**-Zn film after the cell was flushed with fresh ethanol.

respectively.[54,55] Surprisingly, we were unable to find prior reports regarding the transition dipole moment orientation of **F**. However, the transition moment in several xanthene-based dyes (e.g., tetramethylrhodamine, erythrosin B, and eosin Y) has been reported to be aligned within 0 to 20° of the long axis of the xanthene ring structure.[56−58] In Figure 5, we have assumed 0° which makes the angle 75° between the xanthene long axis and the ITO surface normal.

It is important to note that Figure 5 is an incomplete depiction of the trilayer structure. Specifically: (a) We have yet to definitively determine the metal ion coordination environments. (b) ATR only provides information about the polar angle, not the azimuthal angle, which means that we cannot specify the angles between the chromophores. Figure 5 shows only one of the possible bilayer and trilayer geometries. Furthermore, although Figure 5 depicts the ITO as atomically flat, it is not—the rms surface roughness obtained from atomic force microscopy is 0.5 ± 0.1 nm (500 nm × 500 nm scan area).[53,59] Prior studies have shown that as the surface roughness of a substrate increases, the measured tilt angle distribution of an adsorbed molecular film becomes broader and is shifted toward larger angles.[53,59−61] This means that the measured tilt angles listed in Table 1 are somewhat larger than the "true" mean tilt angles.

Transient Absorption Spectroscopy. One of the goals of this work was for the structural information to lend insights to the dynamic processes in the **A**-Zn-**P**-Zn-**F** trilayer-based TTA-UC solar cell.[12] Of the inter-molecule/layer energy and electron transfer events occurring in the TTA-UC trilayer device, singlet energy transfer (i.e., Förster resonance energy transfer or FRET) has perhaps the most readily tangible structural requirements. That is, in addition to the donor emission and acceptor absorption spectral overlap integral (J), refractive index (n), and fluorescence quantum yield of the donor (Φ_D), there are two structural parameters that influence the rate and efficiency (E) of FRET: (a) the donor−acceptor distance (r) and (b) the orientation factor (κ^2), which describes the relative transition dipole orientation of the donor and acceptor molecules (eqs 4 and 5).[62,63]

https://doi.org/10.1021/acs.langmuir.3c01323
Langmuir 2023, 39, 10670−10679

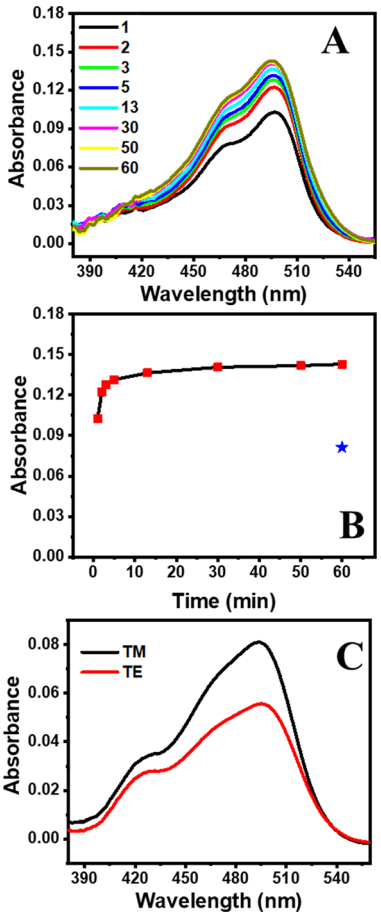

Figure 4. (A) TM-polarized ATR spectra were acquired during the adsorption of **F** to the **A**-Zn-**P**-Zn film, as shown in Figure 3. The spectra were blanked against the spectrum of the **A**-Zn-**P**-Zn film recorded before the **F** solution was injected into the flow cell. The legend indicates the number of minutes that the **F** solution was incubated with the **A**-Zn-**P**-Zn film before the spectrum was acquired. (B) Absorbance at 495 nm vs time obtained from the spectra in (A). The blue star is the absorbance after the cell was flushed with fresh ethanol. (C) TM- and TE-polarized ATR spectra of the **F** layer of the **A**-Zn-**P**-Zn-**F** film after the cell was flushed with fresh ethanol.

$$E = \frac{1}{1 + \left(\frac{r}{R_0}\right)^6} \tag{4}$$

$$R_0 = 9780\,[J\phi_D n^{-4}\kappa^2]^{1/6} \tag{5}$$

Note that R_0 is the Förster radius at which energy transfer efficiency is 50%.

Previously, we attributed the enhanced performance of the **A**-Zn-**P**-Zn-**F** trilayer, as compared to the **A**-Zn-**P** bilayer, to additional absorption by **F** in the optical gap of **P** (i.e., between the Soret and *Q*-band, as shown in Figure S3), followed by near unity ^{1}**F*** to **P** singlet energy transfer.[12] Using time-correlated single photon counting, we provided a low-end estimate of this FRET rate ($k_{FRET} > 2.9 \times 10^{-9}$ s^{-1}) but were inherently limited by the >1 ns instrument response. Here, we performed ultrafast transient absorption (TA) spectroscopy on a mesoporous ZrO_2-**P**-Zn-**F** film to monitor the subnanosecond **F** to **P** energy transfer dynamics (i.e., without **A** to minimize competitive events). As the orientation of **P** does not change upon the adsorption of **F** (Table 1), a bilayer of **F** and

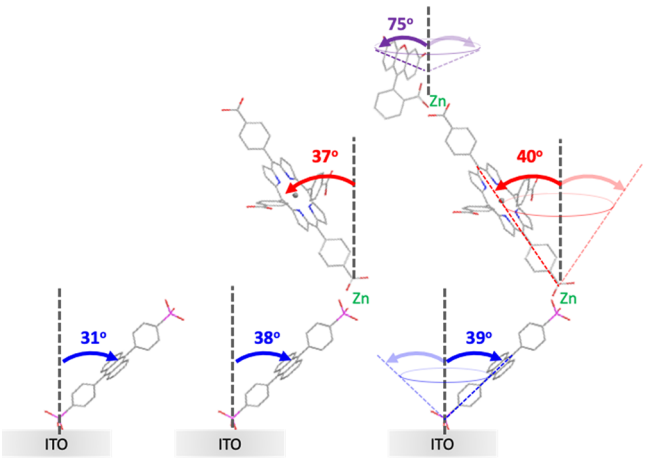

Figure 5. Schematic depictions of the mean polar tilt angles of **A**, **P**, and **F** in the **A** monolayer (left), **A**-Zn-**P** bilayer (middle), and **A**-Zn-**P**-Zn-**F** trilayer (right) on ITO. Since the azimuthal angles are unknown, there is a range of possible angles between the chromophores, and only one possible geometry is shown for the bilayer and trilayer schematics. The light and dark-shaded arrows in the trilayer schematic indicate cones that reflect the range of possible azimuthal angles.

P was used in lieu of the full trilayer to simplify the expected spectral features and still assess the effect of molecular orientation on **F** to **P** energy transfer. Note that these measurements were performed on ZrO_2, rather than ITO, because its relatively high conduction band (E_{cb} = −2.5 V vs NHE) inhibits excited state electron injection into the metal oxide substrate from **F** or **P**.[64] However, our recent study suggests that at high surface coverage, the general structure of the assembly is similar regardless of the nature of the metal oxide.[53] The TA spectra for ZrO_2-**P**-Zn-**F** and ZrO_2-^{3}**P*** were acquired in MeCN to mimic previously used device conditions.[12] The solution spectrum for **F** was acquired in MeOH due to solubility limitations. Also, it is worth noting that out of necessity, mesoporous ZrO_2 was used for the TA measurements, as opposed to planar substrates, to obtain absorbance signals with good S/N.

The TA spectral evolution for the component species, ZrO_2-**P** immersed in MeCN and **F** in MeOH solution, are shown in Figures S4 and S5, respectively. Following direct excitation of ZrO_2-**P**, the long lived excited state absorption (ESA) features in the 450−750 nm region combined with the negative going ground state bleach (GSB) of the *Q*-band at ∼525 nm, are consistent with excitation and rapid intersystem crossing (<500 ps), followed by slow decay (>7 ns acquisition window) of the triplet excited state of **P** (^{3}**P***).[65] Upon excitation of a solution containing **F**, there is a negative going feature at 515 nm that is attributed to both the GSB and stimulated emission (SE) from the singlet excited state of **F** (^{1}**F***),[66] followed by rapid decay with a lifetime of ∼3 ns.

The TA spectra for ZrO_2-**P**-Zn-**F** under preferential excitation of **F** at 475 nm are shown in Figure 6A. Overlayed are the spectra for ^{1}**F*** and ZrO_2-^{3}**P*** (at 0.5 ps) in purple and red, respectively. At the earliest time slice (0.5 ps), there is a negative going signal, not observed in the ZrO_2-**P** sample, which we attribute to GSB/SE of ^{1}**F*** which rapidly decays in <500 ps, resulting in a spectrum that resembles ^{3}**P*** only. We attribute the spectral evolution to excitation of **F** (ZrO_2-**P**-Zn-**F** → ZrO_2-**P**-Zn-^{1}**F***), singlet energy transfer from ^{1}**F*** to **P**

https://doi.org/10.1021/acs.langmuir.3c01323
Langmuir 2023, 39, 10670−10679

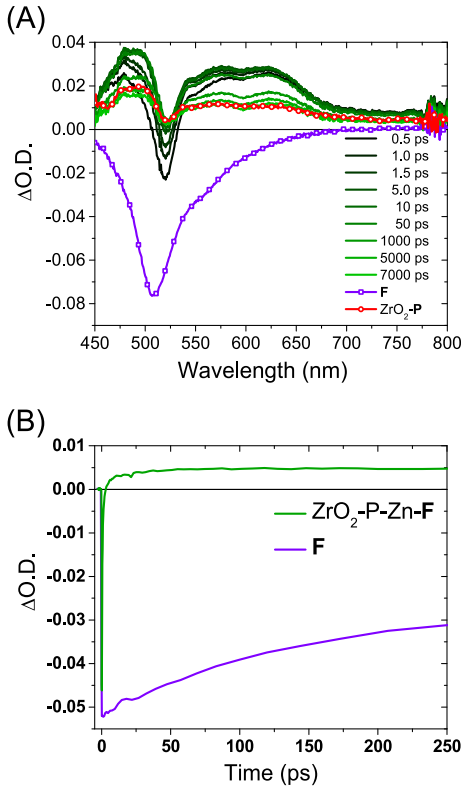

Figure 6. (A) Transient absorbance spectra of ZrO_2-**P**-Zn-**F** films in MeCN following 475 nm excitation. Overlays of TA spectra for **F** in MeOH and ZrO_2-**P** in MeCN at 0.5 ps are shown in purple and red, respectively. (B) Change in absorption at 525 nm for **F** in MeOH and ZrO_2-**P**-Zn-**F** in MeCN (λ_{ex} = 475 nm).

followed by rapid intersystem crossing (ZrO_2-**P**-Zn-^{1}**F*** → ZrO_2-^{3}**P***-Zn-**F**), and then slow decay from the triplet excited state of **P** (ZrO_2-^{3}**P***-Zn-**F** → ZrO_2-**P**-Zn-**F**).

The change in absorption at 525 nm for **F** only and a ZrO_2-**P**-Zn-**F** film excited at 475 nm are shown in Figure 6B. This wavelength was selected to preferentially monitor the **F** decay as there is minimal contribution and/or amplitude change from **P** at 525 nm (Figure S4). As can be seen in Figure 6B, the decay of the GSB/ESA of **F** in ZrO_2-**P**-Zn-**F** occurs within the first 10 ps after the excitation pulse, which is significantly faster than the **F** only solution (Figure S5). The kinetics at 525 nm were fit with a biexponential function (eq 2) and the results are represented by a weighted average lifetime (eq 3), as summarized in Table S2. We found that a single exponential fit was insufficient to capture the kinetics, as is common with molecules bound to mesoporous metal oxides, and is often attributed to inhomogeneities within the film.[67]

Assuming that ^{1}**F*** to **P** energy transfer is the only additional ^{1}**F*** decay mechanism introduced in the ZrO_2-**P**-Zn-**F** film, the FRET rate constant (k_{FRET}) and efficiency (ϕ_{FRET}) can be calculated using eqs 6 and 7:

$$k_{FRET} = \frac{1}{\tau_{F(bl)}} - \frac{1}{\tau_F} \quad (6)$$

$$\phi_{FRET} = 1 - \frac{\tau_{F(bl)}}{\tau_F} \quad (7)$$

where $\tau_{F(bl)}$ and τ_F are the weighted average lifetime of **F** in the bilayer and solution, respectively.[68] From the lifetimes of 15 and 3300 ps for $\tau_{F(bl)}$ and τ_F, respectively, we obtain k_{FRET} = 7 × 10^{10} s^{-1} and ϕ_{FRET} = 99.5%. The >99% efficient energy transfer is consistent with the near unity quenching of **F** emission in the assembly and its notable photocurrent contribution in the TTA-UC solar cell performance.[12] The high energy transfer efficiency can be directly attributed to the ^{1}**F*** to **P** energy transfer rate (7 × 10^{10} s^{-1}) being more than two orders of magnitude faster than the intrinsic excited state decay of **F** ($k_r + k_{nr}$ = 3.3 × 10^8 s^{-1}). In fact, a FRET rate on the order of 10^{10} s^{-1} is on par with some of the fastest singlet energy transfer systems observed to date. Examples include micelles,[69] proteins,[70] peptides,[71] covalent dyads,[72] and other scaffoldings, where much like the metal ion-linked trilayer studied here, the molecules are geometrically constrained in close proximity.

In an attempt to correlate the energy transfer dynamics with the structural information obtained from ATR, we performed rough calculations of the energy transfer efficiency using the FRET eqs 4 and 5. We used J = 2.19 × 10^{-14} cm^6 $mmol^{-1}$, the refractive index of MeCN (n = 1.3), a 91% quantum yield for **F**,[73] and a maximum r of 12 Å (based on the largest sum of Pt−Zn and Zn-center of the xanthene core distances). From the ATR measurements, we fixed the **F** tilt angle at 75° relative to surface normal and to simplify the math, we treated the **P** as having two degenerate perpendicular transition dipole moments at 40° relative to surface normal.[74] Interestingly, when rotating **F** by 1° intervals around the surface normal, all values of κ^2 resulted in energy transfer efficiencies >99%. This suggests that because of the relatively short r, high J, high Φ_D of **F**, and degenerate transition moments of the porphyrin, there is no orientation of metal-ion linked **F** and **P** that would lead to a less than near unity energy transfer efficiency. Consequently, in terms of structure, it is the proximity afforded by the metal-ion linked motif, and not necessarily the orientation, that dictates the **F** to **P** FRET rate in the **A**-Zn-**P**-Zn-**F** trilayer TTA-UC solar cell. Nonetheless, one can envision the orientation being critical for turning on or off FRET in other metal-ion linked chromophore pairs.

SUMMARY AND CONCLUSIONS

We have assembled a metal-ion linked trilayer composed of three different dyes on ITO and demonstrated a method to determine the mean tilt angle of each dye layer relative to the substrate. To our knowledge, this is the first report demonstrating the measurement of the orientation of three different chromophores in a multilayer assembly. TA spectroscopy revealed sub-nanosecond FRET from the third to the second layer, which is responsible for the near unity energy transfer efficiency and improved upconversion solar cell performance. Based on the structural information from ATR and FRET calculations, the rapid interlayer energy transfer is primarily dictated by the proximity between chromophores, meaning that the orientation had minimal effect. Nonetheless, the orientation of each layer in a multilayer composed of different chromophores is a key structural parameter that can influence functional properties such as energy and electron transfer. The ATR approach allows the adsorption of each layer to be monitored in real time, and any changes in the orientation of an underlying layer arising from the adsorption of an overlying layer can be detected. There are some limitations to this method as described herein: (a) The optics and ITO-coated glass substrate presently restrict the wavelength range to the visible and NIR. (b) The single beam

https://doi.org/10.1021/acs.langmuir.3c01323
Langmuir 2023, 39, 10670−10679

geometry requires that the optical alignment be carefully maintained throughout the experiment. (c) As noted above, ATR as implemented herein only provides information about the polar tilt angle, not the azimuthal angle, so the angles between the chromophores are unknown. (d) No information about the distribution of tilt angles about the mean is provided, although the distribution can be obtained using a combination of polarized ATR and total internal reflection fluorescence measurements, as described in earlier publications.[75−77]

■ ASSOCIATED CONTENT

Supporting Information

The Supporting Information is available free of charge at https://pubs.acs.org/doi/10.1021/acs.langmuir.3c01323.

Film preparation conditions and wavelength integration ranges for ATR spectroscopy; UV−vis absorbance spectra of dissolved **A**, **P**, and **F**, ATR spectra of poly(lysine)-405 dye and dextran-rhodamine B films; absorbance spectra of ZrO_2-**P**, ZrO_2-**F**, and ZrO_2-**P**-Zn-**F**; and transient absorbance spectra and biexponential fitting parameters (PDF)

■ AUTHOR INFORMATION

Corresponding Authors

Kenneth Hanson − *Department of Chemistry & Biochemistry, Florida State University, Tallahassee, Florida 32306, United States;* orcid.org/0000-0001-7219-7808; Email: hanson@chem.fsu.edu

S. Scott Saavedra − *Department of Chemistry, University of Arizona, Tucson, Arizona 85721, United States;* orcid.org/0000-0002-9946-2664; Email: saavedra@arizona.edu

Authors

Dhruba Pattadar − *Department of Chemistry, University of Arizona, Tucson, Arizona 85721, United States*

Ashley Arcidiacono − *Department of Chemistry & Biochemistry, Florida State University, Tallahassee, Florida 32306, United States*

Drake Beery − *Department of Chemistry & Biochemistry, Florida State University, Tallahassee, Florida 32306, United States*

Complete contact information is available at: https://pubs.acs.org/10.1021/acs.langmuir.3c01323

Notes

The authors declare no competing financial interest.

■ ACKNOWLEDGMENTS

This work was primarily supported by the Army Research Office under Grant No. W911NF-19-1-0357. Some of the ATR data were acquired in the W.M. Keck Center for Nano-Scale Imaging in the Department of Chemistry and Biochemistry at the University of Arizona. This instrument was supported as part of the Center for Interface Science: Solar-Electric Materials (CIS:SEM), an Energy Frontier Research Center funded by the U.S. Department of Energy, Office of Science, Office of Basic Energy Sciences under Award No. DE-SC0001084.

■ REFERENCES

(1) Paniagua, S. A.; Giordano, A. J.; Smith, O. L.; Barlow, S.; Li, H.; Armstrong, N. R.; Pemberton, J. E.; Brédas, J. L.; Ginger, D.; Marder, S. R. Phosphonic Acids for Interfacial Engineering of Transparent Conductive Oxides. *Chem. Rev.* **2016**, *116*, 7117−7158.

(2) Vilan, A.; Cahen, D. Chemical Modification of Semiconductor Surfaces for Molecular Electronics. *Chem. Rev.* **2017**, *117*, 4624−4666.

(3) Wang, J. C.; Hill, S. P.; Dilbeck, T.; Ogunsolu, O. O.; Banerjee, T.; Hanson, K. Multimolecular assemblies on high surface area metal oxides and their role in interfacial energy and electron transfer. *Chem. Soc. Rev.* **2018**, *47*, 104−148.

(4) Brett, C. M. A. Perspectives and challenges for self-assembled layer-by-layer biosensor and biomaterial architectures. *Curr. Opin. Electrochem.* **2018**, *12*, 21−26.

(5) Lisdat, F.; Dronov, R.; Möhwald, H.; Scheller, F. W.; Kurth, D. G. Self-assembly of electro-active protein architectures on electrodes for the construction of biomimetic signal chains. *Chem. Commun.* **2009**, 274−283.

(6) Zhang, L.; Cole, J. M. Anchoring groups for dye-sensitized solar cells. *ACS Appl. Mater. Interfaces* **2015**, *7*, 3427−3455.

(7) Bugga, P.; Mrksich, M. Dynamic substrates for cell biology. *Curr. Opin. Colloid Interface Sci.* **2018**, *38*, 80−87.

(8) Gooding, J. J.; Parker, S. G.; Lu, Y.; Gaus, K. Molecularly engineered surfaces for cell biology: From static to dynamic surfaces. *Langmuir* **2014**, *30*, 3290−3302.

(9) Senaratne, W.; Andruzzi, L.; Ober, C. K. Self-assembled monolayers and polymer brushes in biotechnology: Current applications and future perspectives. *Biomacromolecules* **2005**, *6*, 2427−2448.

(10) Hanson, K.; Torelli, D. A.; Vannucci, A. K.; Brennaman, M. K.; Luo, H.; Alibabaei, L.; Song, W.; Ashford, D. L.; Norris, M. R.; Glasson, C. R. K.; Concepcion, J. J.; Meyer, T. J. Self-assembled bilayer films of ruthenium(II)/polypyridyl complexes through layer-by-layer deposition on nanostructured metal oxides. *Angew. Chem., Int. Ed.* **2012**, *51*, 12782−12785.

(11) Arcidiacono, A.; Zhou, Y.; Zhang, W.; Ellison, J. O.; Ayad, S.; Knorr, E. S.; Peters, A. N.; Zheng, L.; Yang, W.; Saavedra, S. S.; Hanson, K. Examining the Influence of Bilayer Structure on Energy Transfer and Molecular Photon Upconversion in Metal Ion Linked Multilayers. *J. Phys. Chem. C* **2020**, *124*, 23597−23610.

(12) Zhou, Y.; Ruchlin, C.; Robb, A. J.; Hanson, K. Singlet Sensitization-Enhanced Upconversion Solar Cells via Self-Assembled Trilayers. *ACS Energy Lett.* **2019**, *4*, 1458−1463.

(13) Ogunsolu, O. O.; Murphy, I. A.; Wang, J. C.; Das, A.; Hanson, K. Energy and Electron Transfer Cascade in Self-Assembled Bilayer Dye-Sensitized Solar Cells. *ACS Appl. Mater. Interfaces* **2016**, *8*, 28633−28640.

(14) Ogunsolu, O. O.; Wang, J. C.; Hanson, K. Inhibiting Interfacial Recombination Events in Dye-Sensitized Solar Cells using Self-Assembled Bilayers. *ACS Appl. Mater. Interfaces* **2015**, *7*, 27730−27734.

(15) Beery, D.; Schmidt, T. W.; Hanson, K. Harnessing Sunlight via Molecular Photon Upconversion. *ACS Appl. Mater. Interfaces* **2021**, *13*, 32601−32605.

(16) Bettis, S. E.; Hanson, K.; Wang, L.; Gish, M. K.; Concepcion, J. J.; Fang, Z.; Meyer, T. J.; Papanikolas, J. M. Photophysical characterization of a chromophore/water oxidation catalyst containing a layer-by-layer assembly on nanocrystalline TiO2 using ultrafast spectroscopy. *J. Phys. Chem. A* **2014**, *118*, 10301−10308.

(17) Ding, X.; Gao, Y.; Zhang, L.; Yu, Z.; Liu, J.; Sun, L. Visible light-driven water splitting in photoelectrochemical cells with supramolecular catalysts on photoanodes. *ACS Catal.* **2014**, *4*, 2347−2350.

(18) Dilbeck, T.; Hill, S. P.; Hanson, K. Harnessing molecular photon upconversion at sub-solar irradiance using dual sensitized self-assembled trilayers. *J. Mater. Chem. A* **2017**, *5*, 11652−11660.

(19) Yoshimura, N.; Kobayashi, A.; Genno, W.; Okubo, T.; Yoshida, M.; Kato, M. Photosensitizing ruthenium(ii)-dye multilayers: Photo-

induced charge separation and back electron transfer suppression. *Sustainable Energy Fuels* **2020**, *4*, 3450−3457.
(20) Farnum, B. H.; Wee, K. R.; Meyer, T. J. Self-assembled molecular p/n junctions for applications in dye-sensitized solar energy conversion. *Nat. Chem.* **2016**, *8*, 845−852.
(21) Shan, B.; Vanka, S.; Li, T. T.; Troian-Gautier, L.; Brennaman, M. K.; Mi, Z.; Meyer, T. J. Binary molecular-semiconductor p−n junctions for photoelectrocatalytic CO2 reduction. *Nat. Energy* **2019**, *4*, 290−299.
(22) Ning, H.; Liu, F.; Zhang, T.; Zhao, Y.; Li, Y.; Zhao, Z.; Liu, C.; Zhang, W.; Wang, H.; Li, F. A signal-amplification electrochemiluminescence sensor based on layer-by-layer assembly of perylene diimide derivatives for dopamine detection at low potential. *Anal. Chim. Acta* **2022**, *1214*, No. 339963.
(23) Li, Z. J.; Yao, C. J.; Zhong, Y. W. Near-infrared electrochromism of multilayer films of a cyclometalated diruthenium complex prepared by layer-by-layer deposition on metal oxide substrates. *Sci. China Chem.* **2019**, *62*, 1675−1685.
(24) Zhou, Y.; Ayad, S.; Ruchlin, C.; Posey, V.; Hill, S. P.; Wu, Q.; Hanson, K. Examining the role of acceptor molecule structure in self-assembled bilayers: Surface loading, stability, energy transfer, and upconverted emission. *Phys. Chem. Chem. Phys.* **2018**, *20*, 20513−20524.
(25) Arcidiacono, A.; Robb, A. J.; Masitas, R. A.; Salpage, S. R.; McLeod, G. M.; Chen, J.; Ogunsolu, O. O.; Roper, M. G.; Hanson, K. Inhibited interlayer electron transfer in metal ion linked multilayers on mesoporous metal oxide films. *J. Photochem. Photobiol.* **2022**, *9*, No. 100088.
(26) Ogunsolu, O. O.; Wang, J. C.; Hanson, K. Increasing the Open-Circuit Voltage of Dye-Sensitized Solar Cells via Metal-Ion Coordination. *Inorg. Chem.* **2017**, *56*, 11168−11175.
(27) Robb, A. J.; Miles, D.; Salpage, S. R.; Watson, N.; He, Q.; Wu, Q.; Hanson, K. Role of Metal Ion-Linked Multilayer Thickness and Substrate Porosity in Surface Loading, Diffusion, and Solar Energy Conversion. *ACS Appl. Mater. Interfaces* **2020**, *12*, 38003−38011.
(28) Wang, J. C.; Murphy, I. A.; Hanson, K. Modulating electron transfer dynamics at dye-semiconductor interfaces via self-assembled bilayers. *J. Phys. Chem. C* **2015**, *119*, 3502−3508.
(29) Wang, J. C.; Violette, K.; Ogunsolu, O. O.; Cekli, S.; Lambers, E.; Fares, H. M.; Hanson, K. Self-Assembled Bilayers on Nanocrystalline Metal Oxides: Exploring the Non-Innocent Nature of the Linking Ions. *Langmuir* **2017**, *33*, 9609−9619.
(30) Griffith, M. J.; James, M.; Triani, G.; Wagner, P.; Wallace, G. G.; Officer, D. L. Determining the Orientation and Molecular Packing of Organic Dyes on a TiO2 Surface Using X-ray Reflectometry. *Langmuir* **2011**, *27*, 12944−12950.
(31) McCree-Grey, J.; Cole, J. M.; Evans, P. J. Preferred Molecular Orientation of Coumarin 343 on TiO2 Surfaces: Application to Dye-Sensitized Solar Cells. *ACS Appl. Mater. Interfaces* **2015**, *7*, 16404−16409.
(32) Gliboff, M.; Sang, L.; Knesting, K. M.; Schalnat, M. C.; Mudalige, A.; Ratcliff, E. L.; Li, H.; Sigdel, A. K.; Giordano, A. J.; Berry, J. J.; Nordlund, D.; Seidler, G. T.; Brédas, J.-L.; Marder, S. R.; Pemberton, J. E.; Ginger, D. S. Orientation of Phenylphosphonic Acid Self-Assembled Monolayers on a Transparent Conductive Oxide: A Combined NEXAFS, PM-IRRAS, and DFT Study. *Langmuir* **2013**, *29*, 2166−2174.
(33) Gliboff, M.; Li, H.; Knesting, K. M.; Giordano, A. J.; Nordlund, D.; Seidler, G. T.; Brédas, J.-L.; Marder, S. R.; Ginger, D. S. Competing Effects of Fluorination on the Orientation of Aromatic and Aliphatic Phosphonic Acid Monolayers on Indium Tin Oxide. *J. Phys. Chem. C* **2013**, *117*, 15139−15147.
(34) Sang, L.; Mudalige, A.; Sigdel, A. K.; Giordano, A. J.; Marder, S. R.; Berry, J. J.; Pemberton, J. E. PM-IRRAS Determination of Molecular Orientation of Phosphonic Acid Self-Assembled Monolayers on Indium Zinc Oxide. *Langmuir* **2015**, *31*, 5603−5613.
(35) Katsoukis, G.; Jo, W. J.; Frei, H. Structure and Orientation of Molecular Wires Embedded in Ultrathin Silica Membrane for Artificial Photosynthesis Elucidated by Polarized FT-IRRAS. *J. Phys. Chem. C* **2019**, *123*, 18905−18913.
(36) Lin, H.-C.; MacDonald, G. A.; Shi, Y.; Polaske, N. W.; McGrath, D. V.; Marder, S. R.; Armstrong, N. R.; Ratcliff, E. L.; Saavedra, S. S. Influence of Molecular Orientation on Charge-Transfer Processes at Phthalocyanine/Metal Oxide Interfaces and Relationship to Organic Photovoltaic Performance. *J. Phys. Chem. C* **2015**, *119*, 10304−10313.
(37) Oquendo, L. E.; Ehamparam, R.; Armstrong, N. R.; Saavedra, S. S.; McGrath, D. V. Zinc Phthalocyanine−Phosphonic Acid Monolayers on ITO: Influence of Molecular Orientation, Aggregation, and Tunneling Distance on Charge-Transfer Kinetics. *J. Phys. Chem. C* **2019**, *123*, 6970−6980.
(38) Keszthelyi, T.; Pászti, Z.; Rigó, T.; Hakkel, O.; Telegdi, J.; Guczi, L. Investigation of Solid Surfaces Modified by Langmuir−Blodgett Monolayers Using Sum-Frequency Vibrational Spectroscopy and X-ray Photoelectron Spectroscopy. *J. Phys. Chem. B* **2006**, *110*, 8701−8714.
(39) Gundlach, L.; Szarko, J.; Socaciu-Siebert, L. D.; Neubauer, A.; Ernstorfer, R.; Willig, F. Different orientations of large rigid organic chromophores at the rutile TiO_2 surface controlled by different binding geometries of specific anchor groups. *Phys. Rev. B* **2007**, *75*, No. 125320.
(40) Hill, S. P.; Banerjee, T.; Dilbeck, T.; Hanson, K. Photon Upconversion and Photocurrent Generation via Self-Assembly at Organic−Inorganic Interfaces. *J. Phys. Chem. Lett.* **2015**, *6*, 4510−4517.
(41) Hauptvogel, I. M.; Biedermann, R.; Klein, N.; Senkovska, I.; Cadiau, A.; Wallacher, D.; Feyerherm, R.; Kaskel, S. Flexible and hydrophobic Zn-based metal-organic framework. *Inorg. Chem.* **2011**, *50*, 8367−8374.
(42) https://www.lumiprobe.com/protocols/nhs-ester-labeling. (accessed April 14, 2022).
(43) Lin, H.-C.; Polaske, N. W.; Oquendo, L. E.; Gliboff, M.; Knesting, K. M.; Nordlund, D.; Ginger, D. S.; Ratcliff, E. L.; Beam, B. M.; Armstrong, N. R.; McGrath, D. V.; Saavedra, S. S. Electron-Transfer Processes in Zinc Phthalocyanine−Phosphonic Acid Monolayers on ITO: Characterization of Orientation and Charge-Transfer Kinetics by Waveguide Spectroelectrochemistry. *J. Phys. Chem. Lett.* **2012**, *3*, 1154−1158.
(44) Doherty, W. J., III; Donley, C. L.; Armstrong, N. R.; Saavedra, S. S. A broadband spectroelectrochemical ATR instrument for molecular adlayer studies. *Appl. Spectrosc.* **2002**, *56*, 920−927.
(45) Araci, Z. O.; Shallcross, C. R.; Armstrong, N. R.; Saavedra, S. S. Potential-Modulated Attenuated Total Reflectance Characterization of Charge Injection Processes in Monolayer-Tethered CdSe Nanocrystals. *J. Phys. Chem. Lett.* **2010**, *1*, 1900−1905.
(46) Mendes, S. B.; Bradshaw, J. T.; Saavedra, S. S. Technique for determining the angular orientation of molecules bound to the surface of an arbitrary planar optical waveguide. *Appl. Opt.* **2004**, *43*, 70−78.
(47) Saavedra, S. S.; Reichert, W. M. In situ quantitation of protein adsorption density by integrated optical waveguide attenuated total reflection spectrometry. *Langmuir* **1991**, *7*, 995−999.
(48) Saavedra, S. S.; Reichert, W. M. Integrated optical attenuated total reflection spectrometry of aqueous superstrates using prism-coupled polymer waveguides. *Anal. Chem.* **1990**, *62*, 2251−2256.
(49) Song, W.; Glasson, C. R. K.; Luo, H.; Hanson, K.; Brennaman, M. K.; Concepcion, J. J.; Meyer, T. J. Photoinduced stepwise oxidative activation of a chromophore-catalyst assembly on TiO2. *J. Phys. Chem. Lett.* **2011**, *2*, 1808−1813.
(50) Hotchkiss, P. J.; Jones, S. C.; Paniagua, S. A.; Sharma, A.; Kippelen, B.; Armstrong, N. R.; Marder, S. R. The modification of indium tin oxide with phosphonic acids: Mechanism of binding, tuning of surface properties, and potential for use in organic electronic applications. *Acc. Chem. Res.* **2012**, *45*, 337−346.
(51) Norden, B.; Lindblom, G.; Jonas, I. Linear dichroism spectroscopy as a tool for studying molecular orientation in model membrane systems. *J. Phys. Chem.* **1977**, *81*, 2086−2093.

https://doi.org/10.1021/acs.langmuir.3c01323
Langmuir 2023, 39, 10670−10679

(52) Zheng, Y.; Giordano, A. J.; Shallcross, R. C.; Fleming, S. R.; Barlow, S.; Armstrong, N. R.; Marder, S. R.; Saavedra, S. S. Surface Modification of Indium−Tin Oxide with Functionalized Perylene Diimides: Characterization of Orientation, Electron-Transfer Kinetics and Electronic Structure. *J. Phys. Chem. C* **2016**, *120*, 20040−20048.
(53) Pattadar, D.; Zheng, L.; Robb, A. J.; Beery, D.; Yang, W.; Hanson, K.; Saavedra, S. S. Molecular Orientation of −PO3H2 and −COOH Functionalized Dyes on TiO2, Al2O3, ZrO2, and ITO: A Comparative Study. *J. Phys. Chem. C* **2023**, *127*, 2705−2715.
(54) Gouterman, M. Spectra of porphyrins. *J. Mol. Spectrosc.* **1961**, *6*, 138−163.
(55) Shelnutt, J. A.; Ortiz, V. Substituent effects on the electronic structure of metalloporphyrins: a quantitative analysis in terms of four-orbital-model parameters. *J. Phys. Chem.* **1985**, *89*, 4733−4739.
(56) Lettinga, M. P.; Klarenbeek, E. M.; Zuilhof, H.; Van Zandvoort, M. A. M. J. The Orientation of the Phosphorescence Dipole Moment of Erythrosine B Within Its Molecular Frame. *J. Fluoresc.* **1999**, *9*, 265−279.
(57) Lettinga, M. P.; Zuilhof, H.; Van Zandvoort, M. A. M. J. Phosphorescence and fluorescence characterization of fluorescein derivatives immobilized in various polymer matrices. *Phys. Chem. Chem. Phys.* **2000**, *2*, 3697−3707.
(58) Van Zandvoort, M. A. M. J.; Vossen, D. L. J.; Van Ginkel, G.; Torre, R.; Bartolini, P.; Ricci, M.; Thomas-Oates, J.; Zuilhof, H. Spectral characterization of fluorescent 5- iodoacetamidotetramethylrhodamine and its N-acetylcysteine derivative. *Phys. Chem. Chem. Phys.* **1999**, *1*, 4571−4582.
(59) Ehamparam, R.; Oquendo, L. E.; Liao, M. W.; Brynnel, A. K.; Ou, K.-L.; Armstrong, N. R.; McGrath, D. V.; Saavedra, S. S. Axially Bound Ruthenium Phthalocyanine Monolayers on Indium Tin Oxide: Structure, Energetics, and Charge Transfer Properties. *ACS Appl. Mater. Interfaces* **2017**, *9*, 29213−29223.
(60) Simpson, G. J.; Rowlen, K. L. Quantification of "local" surface orientation: Theory and experiment. *J. Phys. Chem. B* **1999**, *103*, 1525−1531.
(61) Losego, M. D.; Guske, J. T.; Efremenko, A.; Maria, J. P.; Franzen, S. Characterizing the molecular order of phosphonic acid self-assembled monolayers on indium tin oxide surfaces. *Langmuir* **2011**, *27*, 11883−11888.
(62) Forster, T. Energiewanderung und Fluoreszenz. *Naturwissenschaften* **1946**, *33*, 166−175.
(63) Förster, T. Zwischenmolekulare Energiewanderung und Fluoreszenz. *Ann. Phys.* **1948**, *437*, 55−75.
(64) Katoh, R.; Furube, A.; Yoshihara, T.; Hara, K.; Fujihashi, G.; Takano, S.; Murata, S.; Arakawa, H.; Tachiya, M. Efficiencies of Electron Injection from Excited N3 Dye into Nanocrystalline Semiconductor (ZrO2, TiO2, ZnO, Nb2O 5, SnO2, In2O3) Films. *J. Phys. Chem. B* **2004**, *108*, 4818−4822.
(65) Bodedla, G. B.; Dong, Y.; Tang, G.; Zhao, J.; Zhang, F.; Zhu, X.; Wong, W. Y. Long-lived excited states of platinum(ii)-porphyrins for highly efficient photocatalytic hydrogen evolution. *J. Mater. Chem. A* **2022**, *10*, 13402−13409.
(66) Hanczyc, P.; Mikhailovsky, A.; Boyer, D. R.; Sawaya, M. R.; Heeger, A.; Eisenberg, D. Ultrafast Time-Resolved Studies on Fluorescein for Recognition Strands Architecture in Amyloid Fibrils. *J. Phys. Chem. B* **2018**, *122*, 8−18.
(67) Durrant, J. R.; Haque, S. A.; Palomares, E. Towards optimisation of electron transfer processes in dye sensitised solar cells. *Coord. Chem. Rev.* **2004**, *248*, 1247−1257.
(68) Dilbeck, T.; Wang, J. C.; Zhou, Y.; Olsson, A.; Sykora, M.; Hanson, K. Elucidating the Energy- and Electron-Transfer Dynamics of Photon Upconversion in Self-Assembled Bilayers. *J. Phys. Chem. C* **2017**, *121*, 19690−19698.
(69) Mandal, S.; Kuchlyan, J.; Banik, D.; Ghosh, S.; Banerjee, C.; Khorwal, V.; Sarkar, N. Ultrafast FRET to study spontaneous micelle-to-vesicle transitions in an aqueous mixed surface-active ionic-liquid system. *ChemPhysChem* **2014**, *15*, 3544−3553.
(70) Verma, P. K.; Pal, S. K. Ultrafast resonance energy transfer in bio-molecular systems. *Eur. Phys. J. D* **2010**, *60*, 137−156.
(71) Li, H.; Jiang, G.; Jia, M.; Cao, S.; Zhang, S.; Chen, J.; Sun, H.; Xu, J.; Knutson, J. R. Ultrafast Förster resonance energy transfer between tyrosine and tryptophan: potential contributions to protein-water dynamics measurements. *Phys. Chem. Chem. Phys.* **2022**, *24*, 18055−18066.
(72) Patalag, L. J.; Hoche, J.; Holzapfel, M.; Schmiedel, A.; Mitric, R.; Lambert, C.; Werz, D. B. Ultrafast Resonance Energy Transfer in Ethylene-Bridged BODIPY Heterooligomers: From Frenkel to Förster Coupling Limit. *J. Am. Chem. Soc.* **2021**, *143*, 7414−7425.
(73) Magde, D.; Wong, R.; Seybold, P. G. Fluorescence quantum yields and their relation to lifetimes of rhodamine 6G and fluorescein in nine solvents: Improved absolute standards for quantum yields. *Photochem. Photobiol.* **2002**, *75*, 327−334.
(74) Mårtensson, J. Calculation of the Förster orientation factor for donor-acceptor systems with one chromophore of threefold or higher symmetry: zinc porphyrin. *Chem. Phys. Lett.* **1994**, *229*, 449−456.
(75) Edmiston, P. L.; Lee, J. E.; Cheng, S.-S.; Saavedra, S. S. Molecular Orientation Distributions in Protein Films. I. Cytochrome c Adsorbed to Substrates of Variable Surface Chemistry. *J. Am. Chem. Soc.* **1997**, *119*, 560−570.
(76) Runge, A. F.; Mendes, S. B.; Saavedra, S. S. Order parameters and orientation distributions of solution adsorbed and microcontact printed cytochrome c protein films on glass and ITO. *J. Phys. Chem. B* **2006**, *110*, 6732−6739.
(77) Runge, A. F.; Saavedra, S. S.; Mendes, S. B. Combination of polarized TIRF and ATR spectroscopies for determination of the second and fourth order parameters of molecular orientation in thin films and construction of an orientation distribution based on the maximum entropy method. *J. Phys. Chem. B* **2006**, *110*, 6721−6731.

https://doi.org/10.1021/acs.langmuir.3c01323
Langmuir 2023, 39, 10670−10679